Active, Closed-Loop Modulated Turbine Cooling

Vikram Shyam, Dennis Culley, Mark Woike, Jeffrey Eldridge, Scott Jones, Michael Cuy

Purpose

The purpose is threefold: real-time detection of the thermal maps of turbine blades, modular cooling to target particular regions of the hot section based on the real-time thermal maps and a feedback loop to control the modular cooling based on the thermal maps.

Background

The complex cooling scheme within the turbine component has never before been proposed. As with any control system actuation is the only way to affect control. This is particularly difficult in the hot gas path because the temperature is so extreme that every mechanical component is operating at the edge of its material limits. Actuation in this environment is inherently more complex than even the rotating components of the turbine because it requires an active process that implements intentional changes in the flow path during operation.

All actuation devices suffer from limitations. Those that employ moving mechanical components are more affected by temperature fluctuations because of clearance issues between individual parts. Also, the moving mechanical parts have mass therefore the speed of actuation and power required are limited and proportional to the moving mass. Presently, any actuation of the cooling flow in the turbine is done at the compressor exit and is performed by moving a throttle valve with a large mechanical actuator mounted external to the engine core casing. The system is slow and heavy and is only used to make a course cooling flow adjustment based on a predefined schedule.

The actuation devices proposed here are fluidic devices that can be fabricated directly into the mechanical components of the hot gas path. Two types of devices are proposed and they require no moving parts to operate. The first type of device uses the Coanda effect to throttle the cooling air flow along one of two possible paths. The second type of actuator provides a continuously sweeping output flow that improves the film cooling efficiency by improving the film coverage at the blade surface. Both types of actuators effectively eliminate the two main limitations inherent in most mechanical actuation schemes.

The use of thermographic phosphor coatings is well established[1-4] for providing non-contact line-of-sight surface temperature measurements without the drawbacks of uncertain emissivity and interfering reflected radiation that plague optical pyrometer measurements. Surface temperature measurements are obtained from thermographic phosphors either by the temperature dependence of luminescence decay time or temperature dependence of the ratio of luminescence emission at different wavelengths and has been demonstrated for temperature measurements up to 1700°C.[5] Temperatures over 1000°C have been measured from thermographic phosphors directly applied to turbine blades and were successful for both stationary and rotating (low-speed) blades[6]. Luminescence-based temperature sensing overcomes the attachment problem associated with thermocouples and the issues associated with unknown emissivity and interference by stray reflected radiation associated with pyrometry.[1-4] Because of these advantages, thermographic phosphor based temperature measurements have been investigated[6-9] for potential application in turbine engine environments, particularly for engine components coated with thermal barrier coatings (TBCs). In the past, however, luminescence intensity at high temperatures has been insufficient for practical temperature measurements using thermographic phosphors in the highly radiant

turbine engine environment. In particular high-sensitivity, high-resolution surface temperature mapping using imaging techniques has been mostly limited to temperatures below 1000°C[10-13]. Fortunately, a new ultra-bright phosphor was developed during a recent Seedling project that overcomes these limitations by exhibiting retention of ultra-bright luminescence at temperatures above 1000°C[13-14]. This new phosphor, Cr-doped $GdAlO_3$ (Cr:GAP) has been demonstrated to exhibit sufficiently bright luminescence to allow reliable 2D temperature mapping of Cr:GAP-coated surfaces at temperatures above 1000°C. Because luminescence-decay-based temperature mapping avoids the uncertainties associated with thermography or pyrometry (unknown surface emissivities and effects of reflected radiation), this approach was selected as one of two methods investigated for verification and possible feedback for effects of modulated cooling through cooling holes.

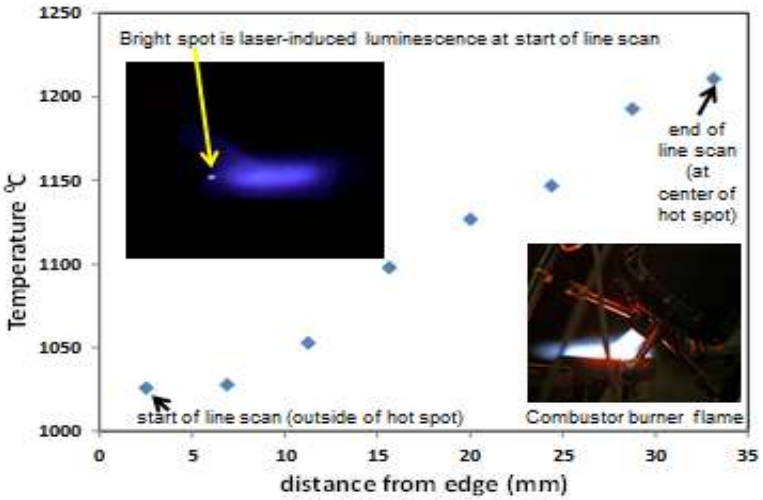

Figure 1. Luminescence based temperature measurements.

The second technique that was investigated as part of this effort was the use of Infrared (IR) Thermography to make blade surface temperature measurements. While IR thermal imaging is a common temperature measurement technique for non-destructive evaluation and other inspection applications, its use to measure blade temperature in a rotating environment for closed loop cooling control in the turbine is innovative. Research efforts to date using this technology have dealt mostly with usage of IR cameras to view external engine components or internal components on large land based turbines, where optical access does not present as challenging of an issue. The use of IR cameras is appealing in that it is a relatively established technology and has the potential to provide the near real time image data that can be used in closed loop cooling control schemes. Long term challenges of using IR technology for this application involve optical access into the engine, viewing enough of the blade for sufficient full-field thermal image, the miniaturization of IR camera technology, and the use of fiber technology to couple the lens to the camera. However, the near term objectives of this present effort was to conduct a coupon level test with an IR camera to test the feasibility of using this technology to make a full-field thermal image of a blade and processing it into a format that would be useable for a closed loop cooling control system. This will be used to assess the current state-of-the-art in IR technology to make a determination on what existing technologies can be folded into this application and what components will need to be developed as a part of a follow-on developmental effort.

Gas turbine engines produce thrust by burning fuel in the combustor and accelerating fluid through the engine. To burn efficiently in the combustor, air entering the engine inlet must be compressed to a high pressure ratio. The fluid exiting the combustor can reach temperatures well in excess of the component thermal limits in the high pressure turbine (HPT) section. Aircraft engines of the future will feature high

operating pressure ratios as well as increased turbine inlet total temperatures. In order to cool the surfaces of components in the HPT, part of the air form the compressor is bled away and fed through internal passages to the HPT where the relatively cooler fluid is injected through discrete holes onto the surface of the hot components. This cooling fluid is deprived of passage through the combustor and moreover, when fed into the rotor, has work done on it by the rotor instead of being used to turn the HPT rotor. In general, an increase in compressor pressure ratio leads to higher engine efficiency. This is accompanied by an increase in the temperature exiting the combustor and entering the high pressure turbine. There are large errors associated with measurement techniques either due to small temperature gradients or invasive measurement methods. The experimental and computational uncertainty leads to excess coolant being used as a safety margin. Up to 12% excess core flow can be used for cooling over the mission of an aircraft jet engine.
Assuming that the surface is adiabatic, a film cooling effectiveness, η, is defined as

$$\eta = \frac{T_\infty - T_{aw}}{T_\infty - T_c}$$

Here, T_{aw} is the adiabatic wall temperature downstream of injection. T_∞ is the freestream temperature. For low speed flows, recovery temperature, T_{rec} can be used instead of freestream temperature. This is useful for finding the effectiveness using an optical method such as infrared thermography. T_c is the coolant exit temperature. Film effectiveness η, is a nondimensional measure of the surface temperature downstream of injection with maximum value of 1.0 for $T_{aw}=T_c$ and minimum value of 0.0 for $T_{aw}=T_\infty$.

It has been noted by industry that in addition to dramatic variations of temperature over a given blade surface, blade-to-blade variations also exist despite identical design. These variations result from manufacturing variations, uneven wear and deposition over the life of the part as well as limitations in the uniformity of coolant distribution in the baseline cooling design. It is proposed to combine recent advances in optical sensing, actuation, and film cooling concepts to develop a workable active, closed-loop modulated turbine cooling system to improve by 10 to 20% the turbine thermal state over the flight mission, to improve engine life and to dramatically reduce turbine cooling air usage and aircraft fuel burn. A reduction in oxides of nitrogen (NOx) can also be achieved by using the excess coolant to improve mixing in the combustor especially for rotorcraft engines. Recent patents filed by industry and universities relate to modulating endwall cooling using valves. These schemes are complex, add weight and are limited to the endwalls. The novelty of the proposed approach is twofold – 1) Fluidic diverters that have no moving parts are used to modulate cooling and can operate under a wide range of conditions and environments. 2) Real-time optical sensing to map the thermal state of the turbine has never been attempted in realistic engine conditions.

Impact on Propulsion system

Figure 2 shows the goals for NASA's Environmentally Responsible Aviation Project, which tracks improvements to aircraft noise, emissions, and fuel consumption as technology progresses. As part of this effort, a study was conducted to determine the improvement in vehicle fuel burn from use of Ceramic Matrix Composites (CMC) in an N+2 turbofan. The N+2 turbofan has a cooled, two-stage high pressure turbine; the cooling flow breakdown is shown in Figure 3. The results of the study are shown in Figure 3, which shows the equivalent reduction in aircraft fuel burn as a function of improvements to both engine thrust-specific fuel consumption and engine weight. Based on this study, the modulated cooling benefit was estimated to be around 0.8%. Unlike CMC airfoils, modulated cooling is assumed to

provide only an engine SFC benefit while not impacting engine weight, thus improving overall aircraft fuel burn by about 2%.

TECHNOLOGY BENEFITS*	TECHNOLOGY GENERATIONS (Technology Readiness Level = 4-6)		
	N+1 (2015)	N+2 (2020**)	N+3 (2025)
Noise (cum margin rel. to Stage 4)	-32 dB	-42 dB	-71 dB
LTO NOx Emissions (rel. to CAEP 6)	-60%	-75%	-80%
Cruise NOx Emissions (rel. to 2005 best in class)	-55%	-70%	-80%
Aircraft Fuel/Energy Consumption‡ (rel. to 2005 best in class)	-33%	-50%	-60%

* Projected benefits once technologies are matured and implemented by industry. Benefits vary by vehicle size and mission. N+1 and N+3 values are referenced to a 737-800 with CFM56-7B engines, N+2 values are referenced to a 777-200 with GE90 engines

** ERA's time-phased approach includes advancing "long-pole" technologies to TRL 6 by 2015

‡ CO_2 emission benefits dependent on life-cycle CO_2, per MJ for fuel and/or energy source used

Figure 2. Fuel burn, emission and noise targets for various generations.

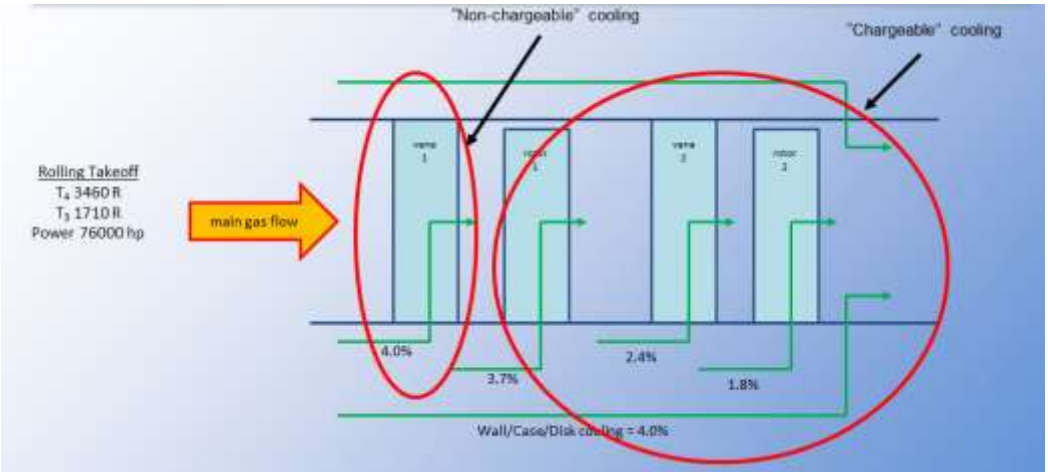

Figure 3. Cooling flow breakdown for N+2 turbofan with cooled, two-stage high pressure turbine

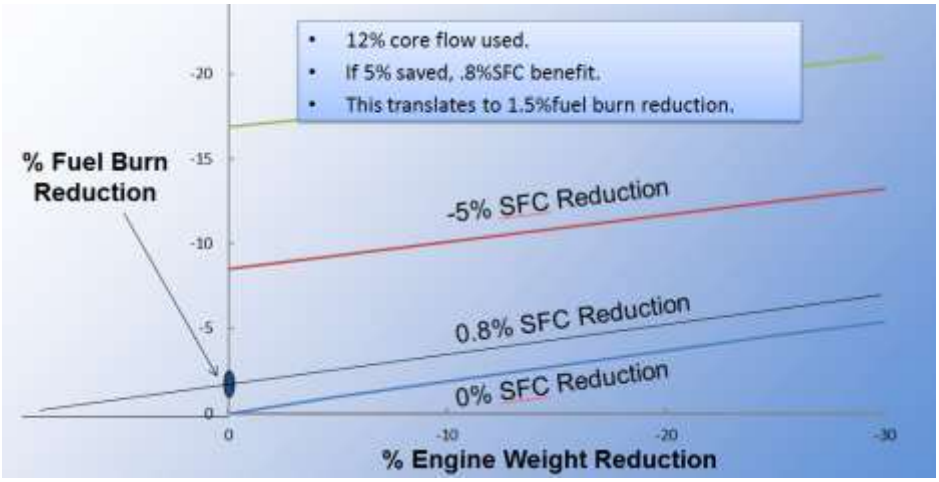

Figure 4. Fuel burn reduction.

Approach

The first part of this work involves detection of the thermal map on turbine blades. The phase 1 effort is comprised of three key components: optical sensing, actuation to control cooling flow and film-cooling circuit design. First, the requirement for accurate, real-time, in situ sensing in the challenging, high-temperature aircraft engine hot section will be addressed through assessment of two methods that have been developed at NASA Glenn – (1) infrared (IR) thermography and (2) luminescence decay from a recently developed Cr-doped gadolinium aluminate thermographic phosphor (pictured in figure 1). For the IR method, a coupon-level test will be conducted to test the ability of this technology to make a full-field thermal image of a blade and process it into a format that would be useable for a closed loop cooling control system. The thermographic phosphor method will entail coupons coated with phosphors that have selected cooling hole patterns. Luminescence-based temperature measurements will be performed with specimens in a furnace and then a burner rig to demonstrate both temperature measurement capability and ability to obtain measurements through a radiant flame. A candidate sensing technique will be downselected at the conclusion of phase 1. Second, the need for accurate, lightweight actuation concepts to provide fine-tuned control of coolant flow rates in individual cooling circuits will be provided by the conceptual design of a system (schematic shown in figure 2) based on fluidic diverter valve technology requiring no moving parts – a key feature considering the engine thermal conditions. This system will minimize cooling flow based on actual need during the mission profile but will revert to maximum cooling flow as a fail-safe condition. A General Electric (GE) proprietary engine schematic will be used to update the cooling design. The resulting design will then be applied to the open Energy Efficient Engine (E3) geometry for publication.

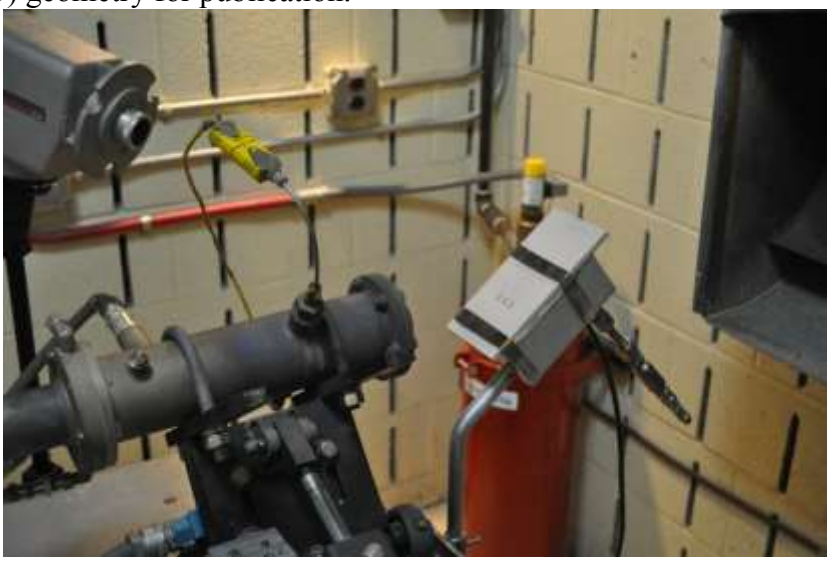

Figure 5. Setup of coupons for infrared thermography in Mach 0.3 burner rig.

Measurement methods

Luminescence decay from a recently developed Cr-doped gadolinium aluminate will be used to determine the surface film effectiveness of a flat plate with film cooling holes. Initial specimens were machined from Rescor 960 high temperature alumina ceramic but these plates were found to have unacceptable thermal shock tolerance. Future plans include producing plates from a Hastalloy X superalloy substrate with bond coat and TBC deposited before the Cr:GAP phosphor coating was deposited. This will provide a layered structure similar to that for actual engine components. Because of the expense of the multilayer deposition required, an interim solution was pursued using a Rescor 902

machinable alumina silicate, which is much tougher than the machinable alumina, and compared to the superalloy substrate, only requires a single layer coating deposition. Rescor 902 plates were acquired and 0.125" diam cooling holes were drilled into the 3"x6" "green" plate before the plates were annealed at 1050°C. Initial testing, without a Cr:GAP surface coating were performed and showed that cracks in the plate formed between 900 and 1000°C. Because of this behavior, testing of Cr:GAP-coated plates is planned for up to but not above 800°C. New, uncracked plates with cooling holes have been sent to Penn State where they are waiting for Cr:GAP coating deposition. Cr:GAP coating deposition will be performed by electron-beam physical vapor deposition (EB-PVD) at an industrial scale coater at Penn State. Deposition of a 25 µm thick Cr:GAP layer will be achieved through electron beam evaporation of a Cr:GAP ingot that had been procured as part of an earlier Seedling project. The plates will be held at a temperature of 1000°C during the deposition.

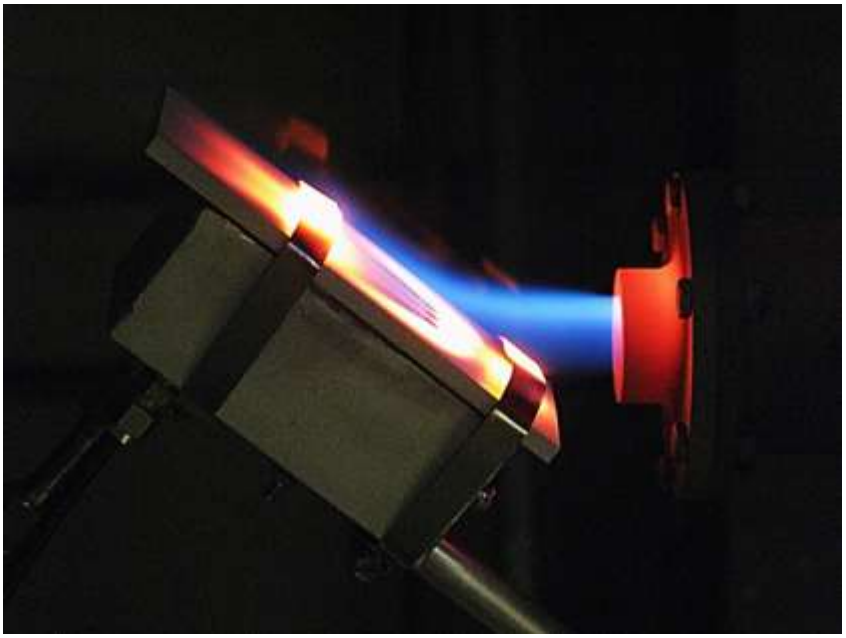

Figure 6. Mach 0.3 burner jet impinging on a coupon.

Testing is performed in the NASA GRC Mach 0.3 Burner Rig facility[16]. This facility is used as an efficient means of subjecting potential aircraft engine/airframe advanced materials to the high temperatures, high velocities and thermal cycling closely approximating actual operating environments. Fixturing was developed for the NASA burner rig so that adjustable cooling air flow could be supplied to pass through the cooling holes in the vane during exposure to the burner rig flame. The sample is held at an angle of approximately 30° from the direction of the burner flame, and cooling air flow is established by mounting the plate against a plenum that could be pressurized to selected values. The pulsed 532 nm excitation laser passed through a 10x beam expander and was positioned to illuminate the area around and downstream of the cooling holes with an illumination diameter approximately 5 cm. The intensified CCD (ICCD) is aligned to be focused on the region illuminated by the excitation laser. The laser Q-switch output pulse was used to synchronize collection of images by the ICCD at the desired delay times after the laser pulse. An 8-µm pyrometer is also aimed just downstream of the leading edge to provide a pyrometer-based temperature measurement for comparison. (see schematic of experimental configuration in figure 7.)

Temperature maps are produced from time-gated images that are collected over a sequence of delay times after the laser pulse, and from this stack of images, a decay time can be determined at each pixel. 2D temperature maps could be produced from a set of background-corrected luminescence images collected over a sequence of gate delays (time between laser pulse and image collection). A stack of images was collected where each image in the stack corresponded to a different gate delay. Therefore, at each pixel in the stack, a luminescence decay curve could be constructed, fitted to determine a decay time, and then converted to temperature by a decay time to temperature calibration.

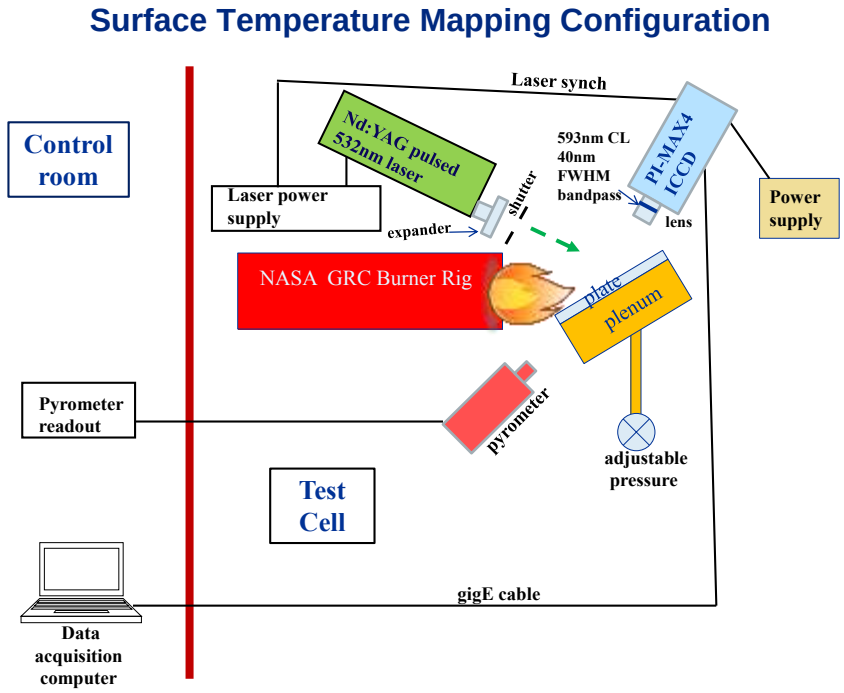

Figure 7. Schematic of luminescence based temperature measurement experiment.

As an example, a temperature map showing the effect of cooling air jet impingement on a laser-heated button specimen is shown in figure 8. Four crossed cooling jets impinged at a glancing angle across the Cr:GAP-coated button specimen which was laser heated to an average surface temperature of 1000ºC. From the 2D temperature map, it is apparent that there was greater air flow from the two nozzles on the left hand side than the two on the right hand side. It is important to note that, unlike pyrometry, this thermal map has the advantage of being insensitive to surface emissivity and reflected radiation.

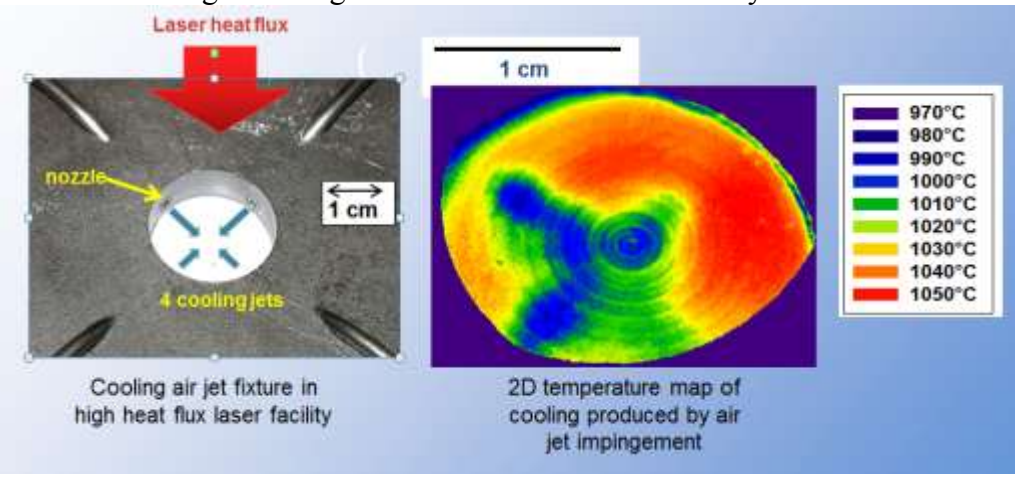

Figure 8. effect of cooling air jet impingement on a laser-heated button specimen

Figure 9. Alumina coupon to be tested in burner rig.

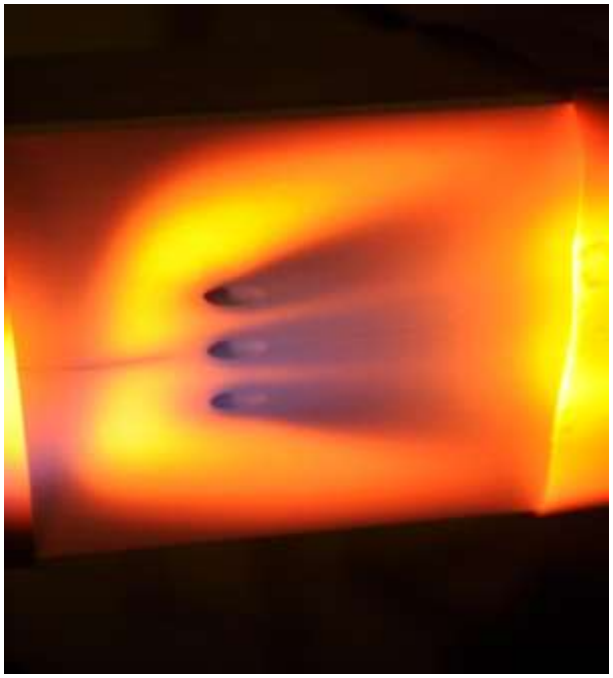

Figure 9

Figure 9 shows the Alumina coupon with 3 cooling holes. Due to the difficulty associated with machining Alumina for high temperature application, several coupons were used to eliminate coupons with crack formations. These coupons will be coated with a thermal barrier coating. The coupons will then be subjected to Mach 0.3 flow at 1200K in the high temperature burner rig of Building 34 at NASA GRC (figure 5). Figure 10 shows an image of the coupon subjected to a 1000K jet. The coolant is provided through the means of a plenum through 3 cooling holes inclined at 30 degrees to the freestream and spaced 3 hole diameters apart. Film effectiveness calculated using this method will be compared to that obtained using an infrared camera. A MATLAB program has been developed to analyze infrared images and to compute the film cooling effectiveness on a film cooled surface. A sample image from infrared thermography of film cooling, taken in NASA GRC's SW-6 facility is shown in figure 11.

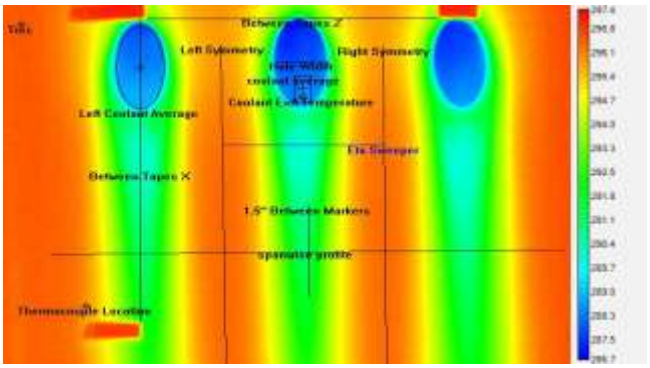

Figure 101. Infrared image of film-cooled flat plate

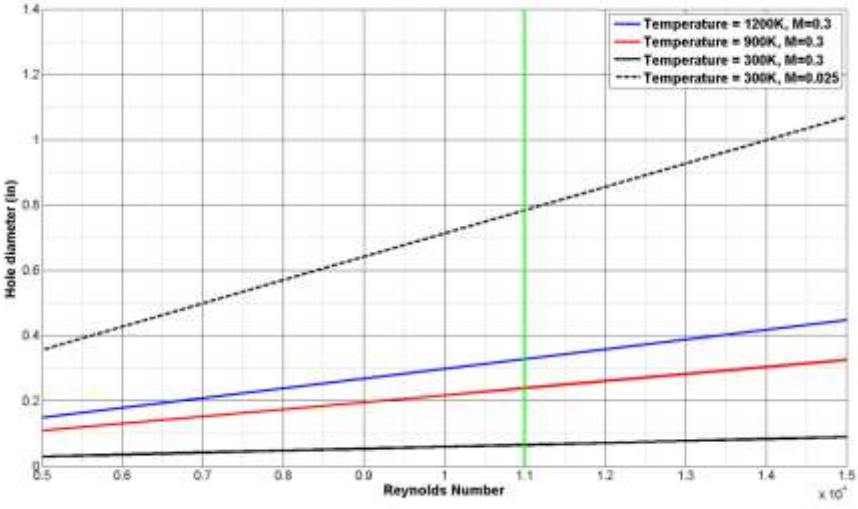

Figure 112. Scaling cooling holes with temperature and Mach number.

Testing using IR Thermography was accomplished using a FLIR SC-650 IR camera. The camera was used to make full field temperature measurements of the test coupon while it was heated to 650°C in the burner rig as a means of accomplishing a preliminary demonstration of the concept. The images acquired at each test condition were processed as follows for use in the closed loop cooling scheme. First, three zones of interest were identified around the cooling holes (for simplicity each hole was assigned to a zone). An average temperature was then calculated for each region. Cooling effectiveness, η, was then calculated for each zone on the IR image using the following calculation described previously:

$$\eta = \frac{T_\infty - T_{aw}}{T_\infty - T_c}$$

Here, T_{aw}, T_∞, T_c are calculated from the temperature values measured on the image. Control would be implemented using cooling efficiency as the control parameter. Each zone is compared to target effectiveness and produces a signal for the feedback mechanism of 0, 1 or 2: 0 means decrease coolant flow, η measured is greater than targeted cooling efficiency, 1 means increase coolant flow, η measured is less than targeted cooling efficiency, 2 means system functioning, do nothing as η measured is with in a pre-defined dead band of the targeted cooling efficiency. Examples of this implementation are shown

in Figure 13. For the proof of concept test this algorithm was intended to be implemented using MATLAB. The long range goal would be to implement the image processing using a FPGA or embedded system. It is envisioned that the interface to the cooling control system would be done using standard digital interfaces (USB, ethernet, etc.). It is realized that implementation of the optics would be more complicated in an actual turbine. The plans would be to use rugged miniature IR cameras and couple to a port in the engine using fiber optics / lens system. The details on this approach would be investigated in the next phase of this effort.

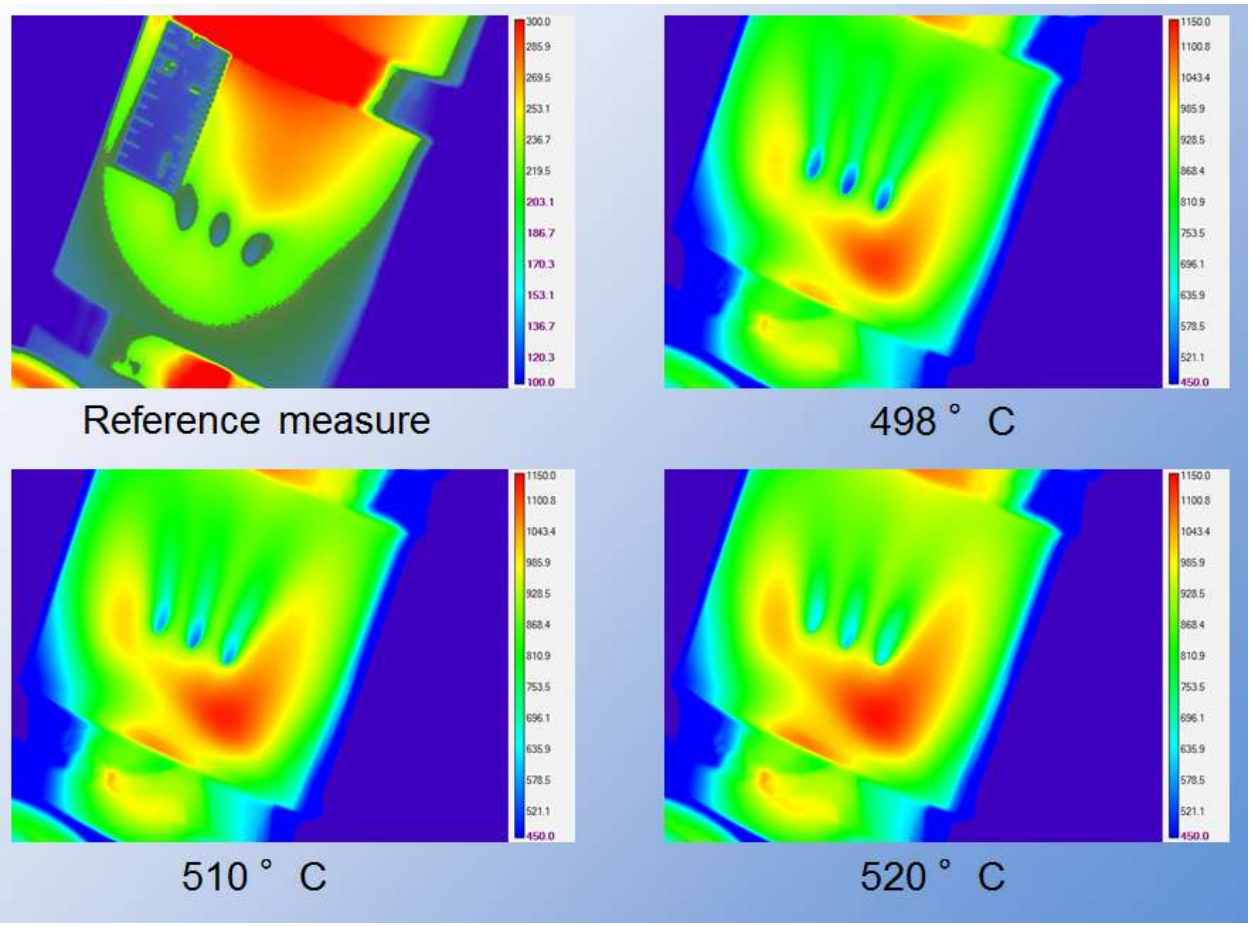

Figure 13. Film cooling coupon at different temperatures to show differing thermal patterns on surface.

Fluidic Network

The fluidic throttle valves[17] are used to apply the appropriate amount of cooling based on the sensed need for cooling at the surface of the turbine blades. The first valve is located at the output of the compressor. Its function is to reduce the bulk cooling flow to the entire hot gas path. Normally this cooling flow consumes at least 20% of the compressor discharge. In operation, the Coanda fluidic valve would immediately return a portion of the secondary air back to the core flow so that it could be used by the turbine to extract work. The Coanda valve is switched by manipulating a very small pressure disturbance within the valve. This pressure may be passive, i.e., extracted directly from pressure signals within the turbine flow path, or they may be provided by a small operator valve at the command of the

control system. As a default, or fail-safe, condition the full cooling flow would be applied although this is normally only the required condition at take-off.

Additional Coanda type fluidic valves can be located to further throttle the cooling flow to appropriate blade rows, or even blades using the same type of operating mechanism. Control of the valves would be dependent on the capability of the sensing mechanism to determine the hot spot locations.

The fluidic actuator located in the turbine blades operates on a different mechanism. The purpose of these devices is to improve the film cooling efficiency by increasing the lateral spread of the film cooling jet on the blade surface. The fluidic actuator performs this function through the nature of the internal flow in the actuator that subsequently produces a sweeping jet at the device output. The device uses no moving parts to create the effect. An array of such devices would be fabricated directly into the mechanical structure of individual turbine blades using an additive manufacturing process.

Figure 14 shows an actuator named F1 with components labeled. Figure 15 shows the functioning of the F1 diverter-type fluidic device that was modelled using Solidworks and printed using a FORTUS 250mc 3D printer. Figure 16 shows the various 3D printed models. Several orifice diameters, channel widths and exit and inlet geometry were studied to determine the sensitivity of the device. The devices were supplied with shop air and allowed to exit onto a level water surface in a 20 gallon aquarium. Videos of the operation of the devices were made for various conditions of the actuator (port 1 closed, port 1 open, port 2 closed, port 2 open.) All possible sequences were attempted and a state map was created to determine the possible modes of operation of the device and to ensure repeatable, consistent control. This effort overlapped with another seedling fund project titled ‘Holistic Aeropropulsion Concepts’.

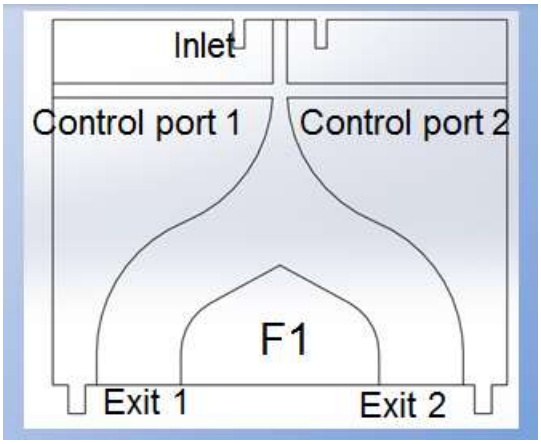

Figure 14. Example of a fluidic diverter, F1.

Figure 125. Fluidic devices tested using additive manufacturing.

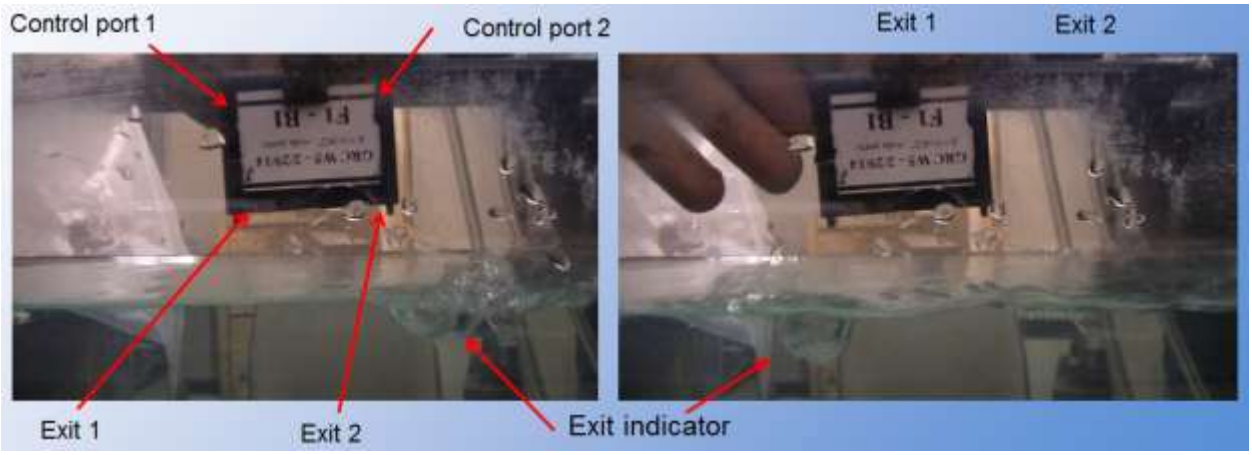

Figure 16. Functioning of a fluidic diverter.

Modulation System

Figure 17 shows a schematic of the modulated cooling scheme. Figure 18 shows the EEE cooling scheme to which this methodology would be applied. The locations of fluidic diverters F0 and F1 are shown along with the percentage of cooling flow that is diverted along each branch. F0 is a simple branching diverter that splits the flow with no switching mechanism. Figure 19 shows the modulated cooling scheme as a flowchart for simplicity. At the turbine level, the cooling flow could be further modulated as shown in figure 20 but such modulation is not the focus of this effort.

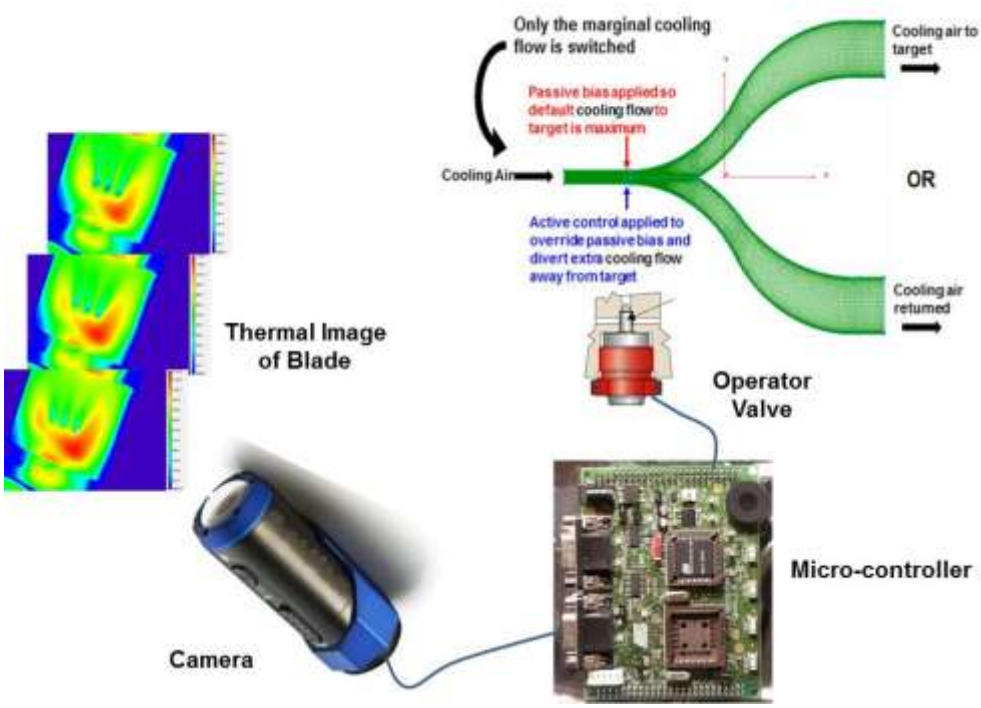

Figure 17. Schematic of modulation system.

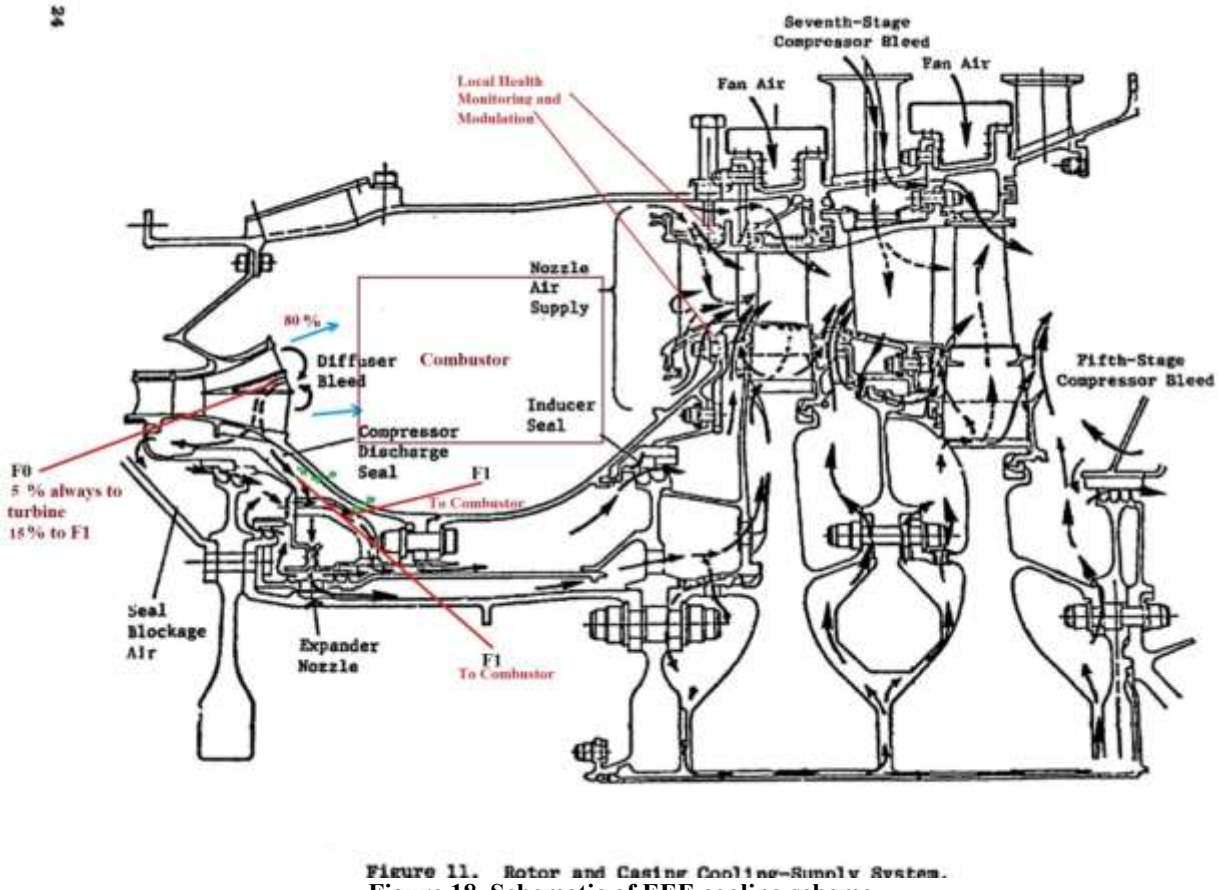

Figure 11. Rotor and Casing Cooling-Supply System.

Figure 18. Schematic of EEE cooling scheme.

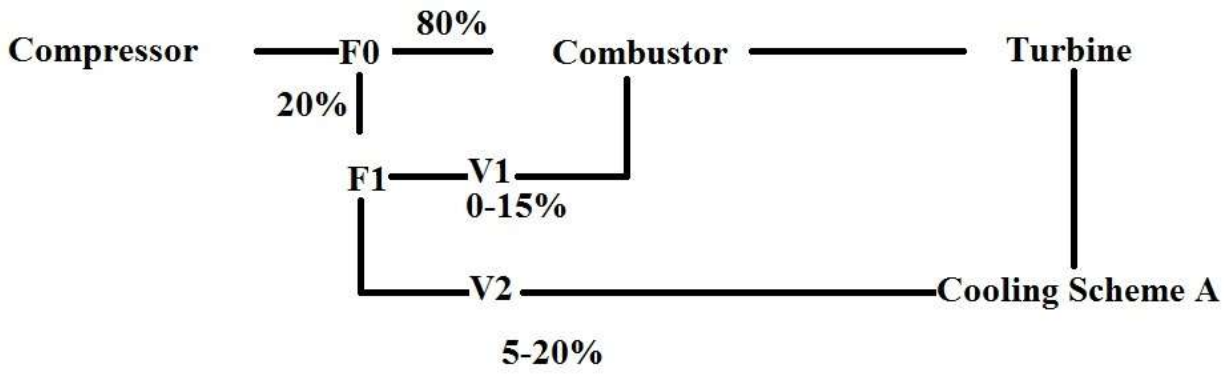

Figure 19. Flowchart of cooling scheme with modulation.

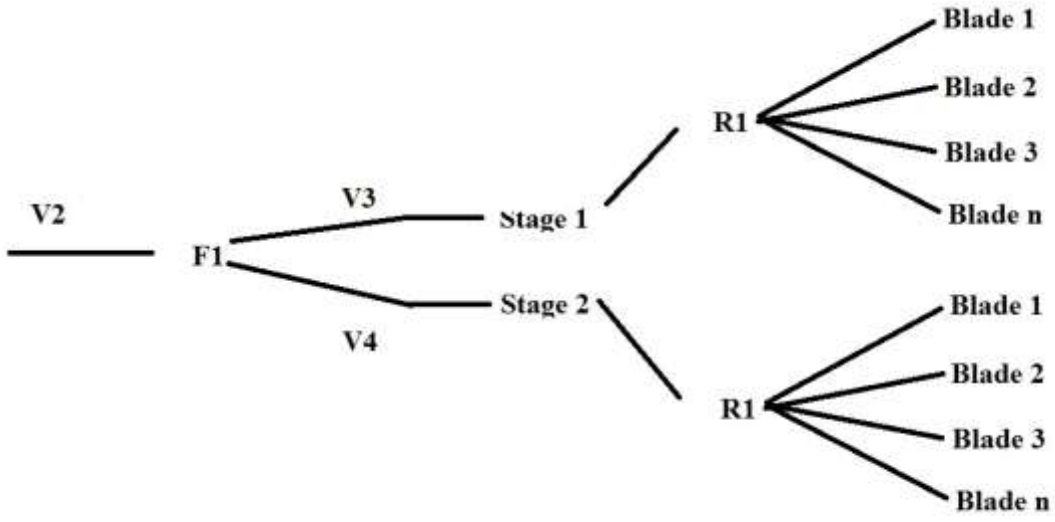

Figure 20. Optional modulation of cooling at blade level.

Figures 21 through 23 show an example of a sequence of events in which the thermal map is used to control the cooling flow through the 3 cooling holes located in the 3 zones. Figure 28 shows the temperature profile downstream of a cooling hole showing regions of blow off near the hole and reattachment downstream. The modulations scheme must be able to recognize such patterns to know whether to increase or decrease the blowing ratio depending on whether or not blow off is detected.

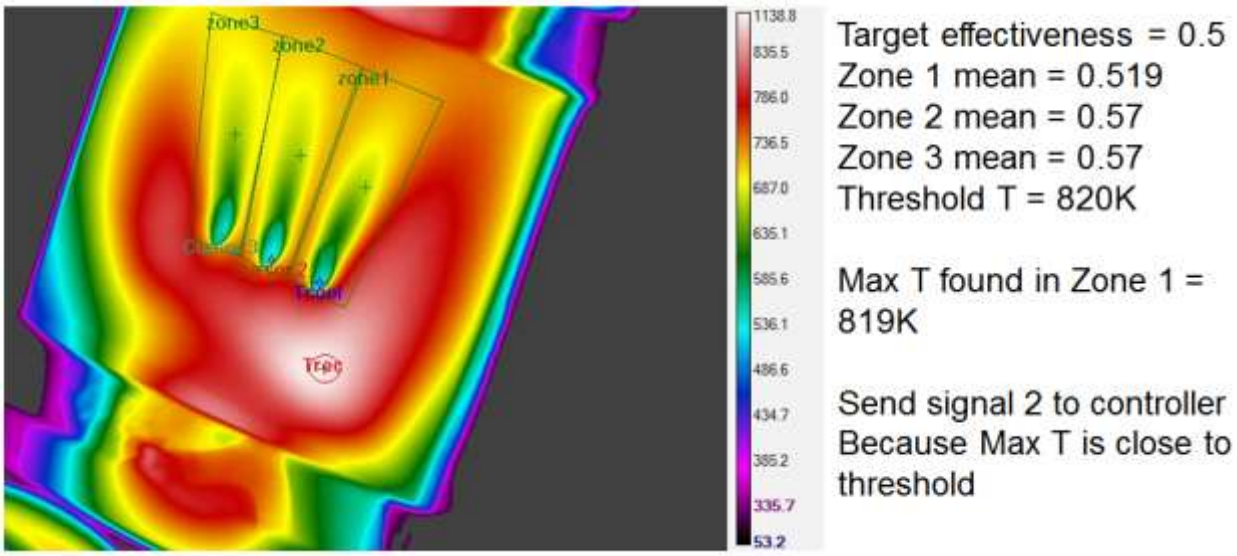

Figure 21. Example 1 of thermal map for modulation control.

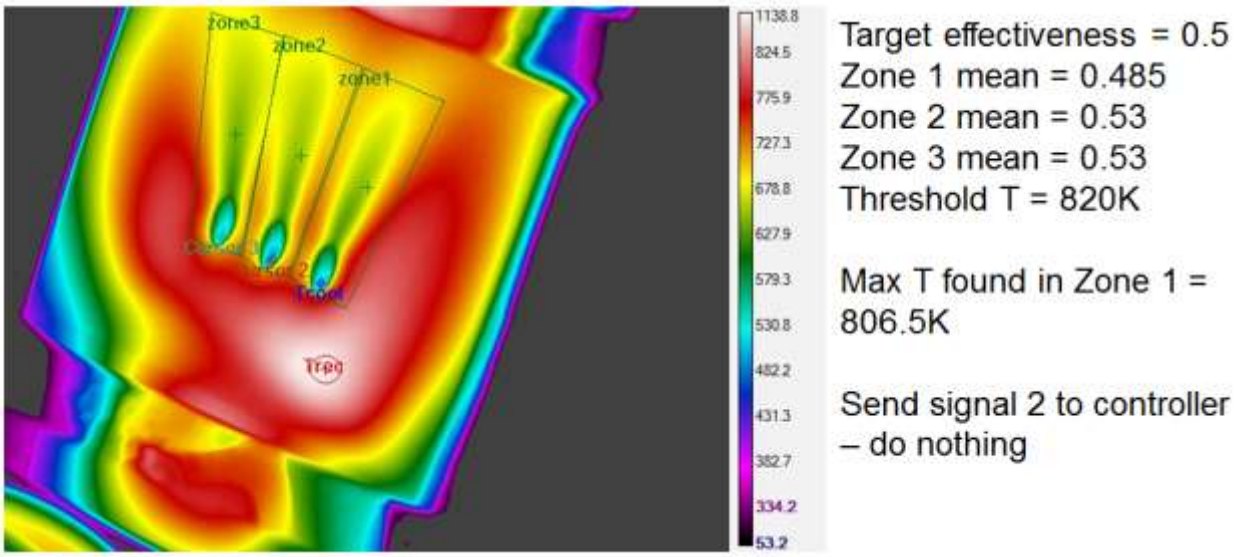

Figure 13. Example 2 of thermal map for modulation control.

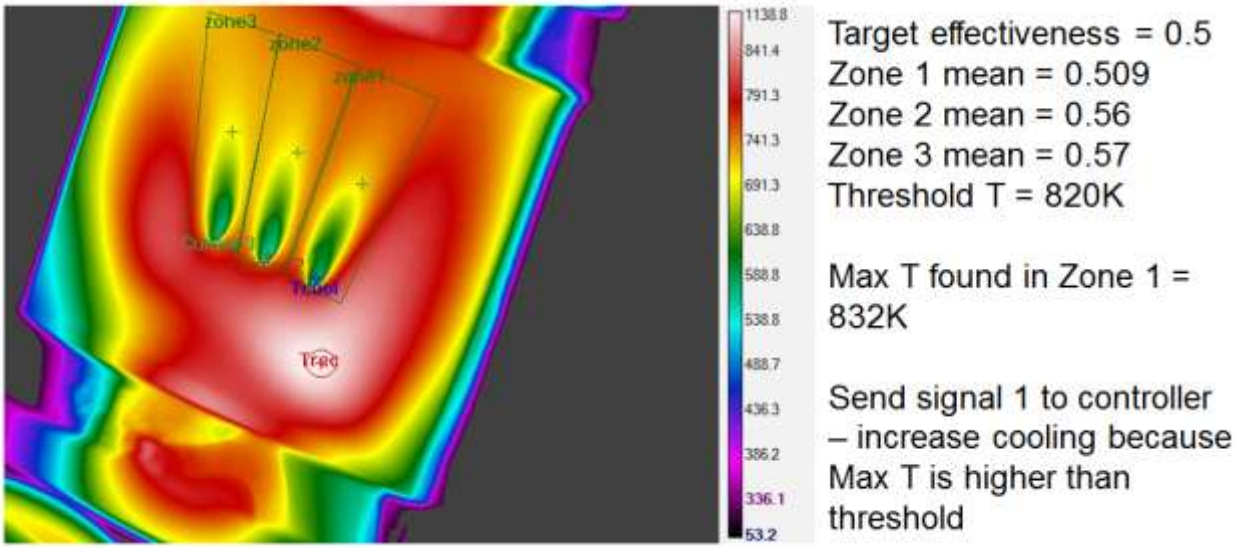

Figure 23. Example 3 of thermal map for modulation control.

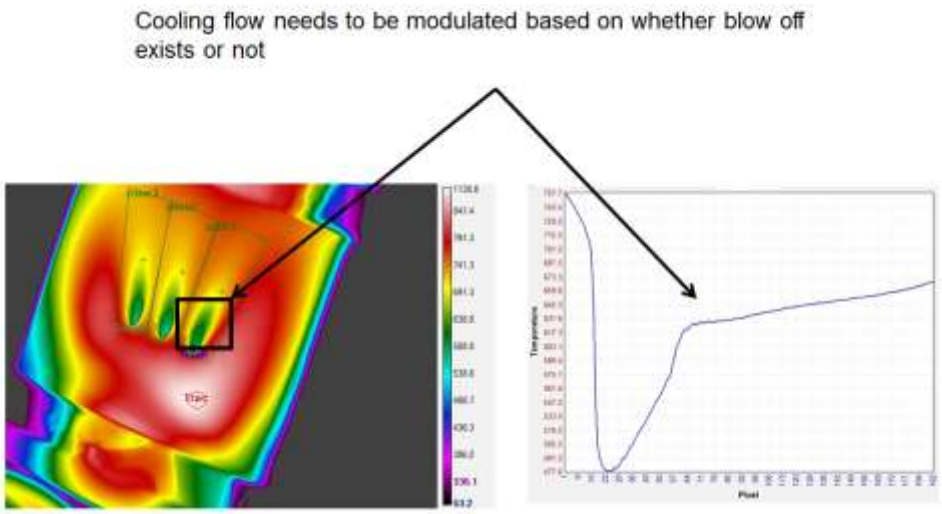

Figure 24. Sample temperature profile downstream of high blowing ratio cooling jet.

Conclusions

A modulation scheme was developed to actively monitor the thermal map of a turbine blade and to control the cooling fraction diverted to turbine cooling. Infrared thermography was used to identify well known cooling effectiveness patterns to show the feasibility of using a thermal map to modulate cooling. Due to difficulties in coating the Hastalloy X coupons, luminescence measurements have not been completed on the coupons as of the writing of this report. These measurements are planned and results will be reported in a subsequent report. Fluidic devices were shown to be predictable and are feasible for use as a control mechanism to divert cooling flow. However, scalability of the fluidic device and sensitivity to engine-realistic environments has not been determined as yet. Considerable work needs to be done to show the feasibility of the overall system.

References

1. S.W. Allison and G.T. Gillies, “Remote Thermometry with Thermographic Phosphors: Instrumentation and Applications,” Rev. Sci. Instrum., 68(7), 2615-2650 (1997).
2. A.H. Khalid and K. Kontis, “Thermographic Phosphors for High Temperature Measurements: Principles, Current State of the Art and Recent Applications,” Senors, 8, 5673-5744 (2008).
3. Brübach, J., Pflitsch, C., Dreizler, A., and Atakan, B., "On Surface Temperature Measurements with Thermographic Phosphors: A Review," Prog. Energy Combust. Sci., 39, 37-60 (2013).
4. Chambers, M. D., and Clarke, D. R., "Doped Oxides for High-Temperature Luminescence and Lifetime Thermometry, Annu. Rev. Mater. Res. 39, 325-359 (2009).
5. M.R. Cates, S.W. Allison, S.L. Jaiswal, and D.L. Beshears, “YAG:Dy and YAG:Tm Fluorescence to 1700°C,” 49th International Instrumentation Symposium - The Instrumentation, Systems, and Automation Society, Orlando, Florida, May, 2003.
6. K.W. Tobin, S.W. Allison, M.R. Cates, G.J. Capps, D.L. Beshears, M. Cyr, and B.W. Noel, “High-Temperature Phosphor Thermometry of Rotating Turbine Blades,” AIAA J., 28(9), 1485-1490 (1990).
7. Steenbakker, R.J.L., Feist, J.P., Wellman, R.G., and Nicholls, J.R., "Sensor Thermal Barrier Coatings: Remote In Situ Condition Monitoring of EB-PVD Coatings at Elevated Temperatures," J. Eng. Gas Turb. Power, 131, 041301-1 to 041301-9 (2009).
8. Gentleman, M.M. and Clarke, D.R., "Concepts for Luminescence Sensing of Thermal Barrier Coatings," Surf. Coat. Technol., 188-189, 93-100 (2004).
9. Eldridge, J.I., Bencic, T.J., Allison, S.W., and Beshears, D.L., "Depth-Penetrating Temperature Measurements of Thermal Barrier Coatings Incorporating Thermographic Phosphors," J. Therm. Spray Technol., 13(1), 44-50 (2004).
10. Aldén, M., Omrane, A., Richter, M., and Särner, G., "Thermographic Phosphors for Thermometry: A Survey of Combustion Applications," Prog. Energy Combust. Sci., 37, 422-461 (2011).
11. Seyfried, H., Särner, G., Omrane, A., Richter, M., Schmidt, H., and Aldén, M., "Optical Diagnostics for Characterization of a Full-Size Fighter-Jet Afterburner," ASME Turbo Expo 2005, GT2005-69058, 813-819 (2005).
12. Omrane, A., Ossler, F., and Aldén, M., "Temperature Measurements of Combustible and Non-Combustible Surfaces Using Laser Induced Phosphrescence," Exp. Ther. Fluid Sci., 28, 669-676 (2004).
13. Fuhrmann, N., Schneider, M., Ding, C.-P., Brübach, J., and Dreizler, A., "Two-Dimensional Surface Temperature Diagnostics in a Full-Metal Engine Using Thermographic Phosphors," Meas. Sci. Technol., 24, 095203 (2013).
14. Eldridge, J.I. and Chambers, M.D., "Temperature Sensing Above 1000 C using Cr-Doped GdAlO3 Spin-Allowed Broadband Luminescence," in Temperature: Its Measurement and Control in Science and Industry, Vol 8, AIP Conf. Proc. 1552, 873-878 (2013).
15. Eldridge, J.I. and Chambers, M.D., Temperature and Pressure Sensors Based on Spin-Allowed Broadband Luminescence of Doped Orthorhombic Perovskite Structures, U.S. Patent 8,695,430, Apr 15, 2014.
16. Dennis S. Fox, Robert A. Miller, Dongming Zhu, Michael Perez, Michael D. Cuy, and R. Craig Robinson, “Mach 0.3 Burner Rig Facility at the NASA Glenn Materials Research Laboratory,” NASA TM 2011-216986.
17. Raghu, S. & Raman, G. (1999) Miniature fluidic devices for flow control. ASME FEDSM 99-7256.